Pulse-Echo Harmonic Generation Measurements for Non-Destructive Evaluation

S.R. Best, A.J. Croxford, S.A. Neild

October 3, 2013

Abstract

Ultrasonic harmonic generation measurements have shown promising potential for detecting nonlinear changes in various materials. Despite this, the practical implementation of the technique in non-destructive evaluation (NDE) has typically been limited to the through transmission setup case, with which problems arise in certain situations. Recently, works in the fields of nonlinear fluids and biomedical imaging have reported different application of the harmonic generation theory by making use of reflective boundaries and beam focusing. It is thought that such techniques may be similarly applied in the field of NDE to enable single-sided nonlinear inspection of components. In this paper, we initially describe a numerical model which has been used to determine the effects of attenuation and acoustic beam diffraction on measurements of the nonlinear parameter β. We then extend the model to incorporate first the effects of multiple reflecting boundaries in the propagation medium, then of focused source excitation. Simulations, supported by experimental data, show that nonlinear pulse-echo measurements have the potential to provide a viable (and more practical) alternative to the usual through-transmission type as a means of measuring β in solids. Furthermore, it is shown that such measurements may by optimised by focusing the acoustic source at a certain point relative to the specimen boundary.

1 Introduction

Bulk harmonic generation measurements have been used for many years to determine nonlinearity parameters in various different types of materials. In the field of nondestructive evaluation (NDE), this is particularly useful as it allows us to monitor the early signs of damage developing in critical components. In recent years, many papers have reported increasing levels of nonlinearity in test specimens subjected to creep and fatigue processes - see, for example, Refs. [1, 2, 3, 4]. Such studies have typically used a through-transmission setup to measure the baseline nonlinearity in the undamaged state, then monitored the change, using the same setup, as the specimen has undergone fatigue cycling. The usual method for extracting the nonlinear parameter, β, from the raw ultrasonic data, is the well-known plane wave expression:

$$\beta = \frac{8}{k^2 x} \frac{A_2}{A_1^2} \tag{1}$$

Here, k is the excitation frequency used to interrogate the specimen, x is the distance of propagation, and A_1 and A_2 are the extracted amplitudes of the fundamental and second harmonic components, respectively, from the received signal. Eq. (1) has proven effective for measuring relative changes in β when a component is monitored in an in-situ manner using constant experimental conditions. One

of the associated drawbacks, however, is that it is likely not to fully represent the true conditions of measurement, when factors such as beam diffraction and attenuation are taken into account. As a result of this, absolute β measurements made using Eq. (1) are not a precise representation of the actual nonlinearity of a specimen. This fact also makes it difficult to compare two measurements made using different experimental parameters (for example frequency, propagation distance), as they may be inaccurate to different degrees. These points were explored in recently published work by the authors [5], where it was proposed that thorough modelling of the experimental conditions could afford more accurate and comparable measurements of β. A large part of the referenced work was the development of a numerical model designed to capture the nonlinear behaviour in a diffractive sound beam - the first part of this work outlines and expands upon the model.

From a practical point of view, a limitation of using Eq. (1) to determine β is that is depends upon measurements being made in the through-transmission configuration, with transmitter and receiver located on opposite surfaces of the specimen. While generally not a problem in a laboratory environment, this fact may be restricting in a field measurement scenario where, for example, access is only possible to the outer surface of a component. In this situation, it would be ideal to make use of a pulse-echo configuration to make a single-sided measurement. Complications arise here however, as a result of the presence of the reflecting interface. Specifically, it is known that the pressure-release boundary type present at a free surface is known to destructively alter the nonlinear generation process. It is not immediately obvious therefore, whether it may be possible to make pulse-echo measurements involving reflection from a free boundary. This work therefore primarily aims to assess the feasibility of making such measurements.

Examples of both theoretical and experimental work on the reflection of second harmonics can be found in the literature. Most of these, however, have been found in the fields of biomedical imaging [6, 7, 8] and fluid nonlinearity [9, 10], which has generally meant that rigid-type reflectors have been considered. Here the emphasis is on the type of pressure-release interface which typically features in the pulse-echo inspection of a solid component. Some fluid-based works in the literature [10, 11] have also featured the combined use of boundaries and focused acoustic sources as a means of optimising the measurement system. It is thought that similar principles could be applied to solids, and we address this idea in the later sections.

In Section 2, we outline the elements of the numerical harmonic generation model developed in previously published work [5]. This model combines the effects of nonlinearity, diffraction, and attenuation in order to describe second harmonic accumulation in the beam of a finite acoustic source. The model is then expanded upon in Section 3 to incorporate the effects of multiple reflections from free boundaries. Simulated predictions are compared with with results of experimental tests in Section 4. Then, in Sections 5 and 6, we explore the optimisation of the pulse-echo configuration, firstly by altering the input frequency, and then by using beam focusing. A summary and conclusions of the work are presented in Section 7.

2 Modelling a Diffractive Sound Beam

Numerical modelling provides the most efficient means of accurately capturing the nonlinear behaviour of a diffractive three-dimensional sound beam. It also enables the input parameters to be matched to those of any given practical setup. In the context of fluids, the most widely-used modelling scheme is the Kokhlov-Zabolotskaya-Kuznetsov (KZK) equation, derived by Zabolotskaya and Kokhlov (1969) [12], and Kuznetsov [13] (1971). This is an augmentation of the Burgers equation, and combines the effects of diffraction, nonlinearity, and absorption in directional sound beams. Many solutions to this equation [14, 15] are relevant to propagation in fluids, where nonlin-

earity levels are generally high. As such, the computations retain large numbers of higher harmonics in the calculations and can be time consuming to implement. One advantage of modelling propagation in solids is that nonlinearity levels are relatively low, which enables us to adopt a quasi-linear approximation. In this sense, we consider only the first two order terms of excitation - those of the fundamental and second harmonic. The framework presented below is therefore equivalent to quasi-linear solutions of the KZK equation as described in Refs. [16, 17].

In the quasi-linear scheme, the generation of second harmonics in a sound beam can be visualised as the excitation and re-emission of a volume distribution of virtual nonlinear sources [17]. An assumption is that the beam of acoustic energy is reasonably well confined to the axis of propagation, a condition known as the parabolic (or quasi-optical) approximation. As an underlying equation, we use that of Ingenito and Williams [18] (see Eq. (11) therein), derived by imposing the condition of large ka (where k and a are the excitation wave number and transmitter radius, respectively) upon the nonlinear wave equation. The resulting simplified solution can be expressed in terms of Green's functions, and describes the summation of contributions from all virtual nonlinear sources in the domain of wave propagation:

$$U_2(x,y,z) = C\int_0^Z \int_{-Y}^{Y} \int_{-X}^{X} U_1^2(x',y',z')G(x,y,z|x',y',z')dx'dy'dz' \tag{2}$$

Here, $U_2(x,y,z)$ is the nonlinear displacement amplitude at the target point (x,y,z) of interest, denoted by standard Cartesian coordinates, where x and y are transverse to the source plane, and z is the direction of propagation. $U_1(x',y',z')$ is the local linear displacement amplitude of a virtual source at (x',y',z') with volume dx',dy',dz'. $G(x,y,z|x',y',z')$ is then the Green's function describing propagation of the nonlinear wave from the virtual source to the target:

$$G = (1/R)\exp(2ikR - \alpha_2 R) \tag{3}$$

where R is the distance between the two points,

$$R = [(x-x')^2 + (y-y')^2 + (z-z')^2]^{1/2}, \tag{4}$$

and α_2 is the attenuation coefficient at the second harmonic frequency. The values X, Y and Z in Eq. (2) represent the integration limits along the respective axes. The constant of proportionality, $C = k^2\beta/(2\pi c_l)$, (where c_l is the longitudinal sound speed), is found by swapping the fluid nonlinear parameter found in the original equation [18] with that for solids, as defined by Beyer [19].

2.1 Numerical Implementation

To solve Eq. (2), a numerical algortihm was developed in Matlab®. To reduce memory requirements, the three-dimensional integration is performed in stages; Fig. 1 shows a schematic diagram to illustrate this process.

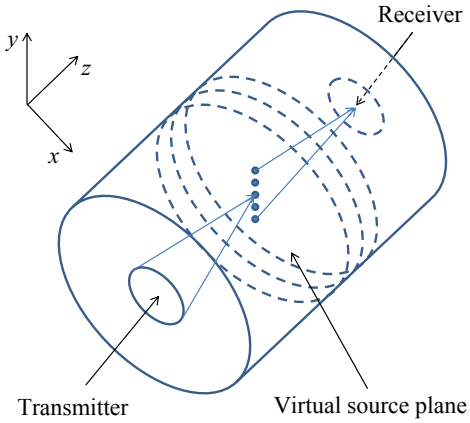

Figure 1: Schematic to illustrate the numerical integration process

The propagation domain is divided into planes of virtual sources parallel to the transducer plane. Initially, the linear displacement amplitudes are calculated for all points in a plane using the Rayleigh-Sommerfeld diffraction integral. This stage of the computation is carried out using the algorithm of Zemanek [20], which is modified slightly to include a linear attenuation coefficient. The linear displacement amplitudes are then squared and multiplied by the appropriate Green's functions for the target point, before summing. This process is repeated for the next virtual source plane, and the contributions are added in sequence. In order to correct the amplitudes for a finite-radius receiver, the field averaging for the both the fundamental and second harmonic is calculated as follows:

$$U_{1,2}(0,0,z) = \frac{1}{\pi b^2} \int_0^b U_{1,2}(x,0,z) 2\pi x dx \tag{5}$$

where b is the radius of the receiver - here the axial symmetry of the system is exploited. Earlier references to this so-called diffraction-correction can be found in the literature [21, 22].

As described thus far, this model is a valid representation of the through-transmission type measurement, in which a finite circular transmitter and receiver are located on opposite sides of the medium. In the aforementioned work [5], experimental results from through-transmission tests are provided in support of the numerical predictions, which show reasonably good agreement. The numerical framework provides a basis which can be readily expanded upon to represent different measurement scenarios. In the next sections, we describe the extensions made to the model to incorporate the effects of reflecting boundaries and beam focusing.

3 Incorporating Reflecting Boundaries

As mentioned previously, the complication associated with making nonlinear pulse-echo inspections is the effect of the reflecting boundary on the accumulation of harmonics over the course of the round trip. It was noted much earlier by Fay [23] that at an interface, a reflected wave can be seen as a similar, but oppositely directed wave to that incident. In the case of a rigid reflector (for example, a gas-solid boundary), the incidental and reflected waves are identical and coincide. If however, the reflector is not rigid, instabilities can occur between the different harmonic components of a nonlinearly propagating wave. Fay concluded that in the case of a pressure-release boundary (e.g. a solid-vacuum interface), the 'least stable' waveform is produced - that is, the maximum possible instability between the harmonic components exists. This was later confirmed experimentally

by Breazeale and Lester [24], who performed experiments in water with different type interfaces, and noted a reversal in the distortion of a nonlinear wave after reflection from a pressure-release boundary. Similar behaviour was then noted by Thompson et al. [25] from their experiments in silica and aluminium. The behaviour of the harmonic components was attributed by Van Buren and Breazeale [26], [27] to phase changes occuring at the pressure-release boundary. Assuming independent reflection of the harmonic components, the fundamental and second harmonic each undergo a phase shift of 180^o, equivalent to a switch in sign. Due to the different wavelengths of the components, a relative phase change occurs, which is maintained upon subsequent propagation away from the boundary. Now however, the reflected linear component generates a new second harmonic with the original 'correct' phase relationship, which leads to cancellation with the reflected second harmonic. Buck and Thompson [28], and more recently Bender [29] have also noted that in the one-dimensional (plane wave) case with no attenuation included, the harmonic component generated during forward propagation will theoretically diminish to zero on returning to its origin after reflection from the free boundary. Evidently, the implications of this finding could rule out the possibility of using a pulse-echo configuration to make harmonic generation measurements. It should be stressed, however, that this result is arrived at by using the plane wave analysis. Our aim here therefore, is to investigate the implications of applying a three-dimensional treatment to the problem.

Similar previous work exists in this area for the case when a boundary is present. This includes the work of Garrett et al. [6], who expanded upon the quasi-linear parabolic theory of Naze Tjotta and Tjotta [30] to develop a reflection theory for nonlinear parametric radiation. The numerical predictions of their model compared reasonably well with results of experiments performed in water, using a polyfoam target as the reflector. Makin et al. [31] have also presented analytical solutions based on the use of focused Gaussian beams, designed to demonstrate the effects of a curved interface. Other uses of three-dimensional models in the context of fluids can also be found [9, 11].

Here, the focus is on second harmonic generation from a planar, radially symmetric source radiating into a solid with a planar free boundary. We extend the numerical model described in the previous section such that the excitation may undergo an unlimited number of round-trips inside a solid specimen with a free interface at either side. This may then be applied more directly to the case of a pulse-echo inspection. To help visualise the problem, we unfold the geometry such that propagation after reflection from the boudary at z_{bound} is equivalent to continued propagation in the positive z-direction. Fig. 2 shows a schematic to illustrate this, where the space is divided into regions separated by the locations of the reflecting boundaries.

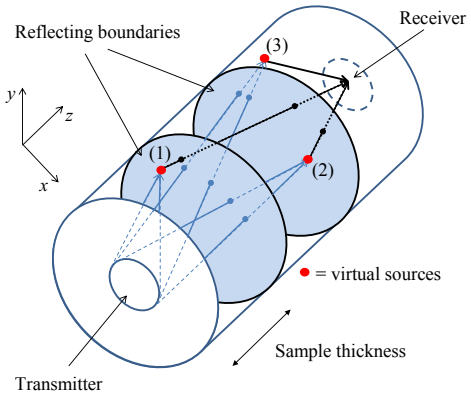

Figure 2: Schematic to illustrate the numerical integration process over multiple boundary-separated regions.

Specifically, Fig. 2 corresponds to the case of an excitation undergoing double reflection - once at the far boundary, once at the boundary of origin - followed by reception at the far boundary. In order to sum nonlinear contributions throughout the entire space, each must be modified according to the position of the associated virtual source relative to the target point. To express this mathematically, we modify Eq. (2) to include a reflection coefficient term:

$$U_2(x,y,z) = C\int_0^Z \int_{-Y}^{Y} \int_{-X}^{X} U_1^2(x',y',z',)R(z,z')dx'dy'dz' \tag{6}$$

Here, the reflection term $R(z,z')$ is determined by the axial positions of the virtual source, z', and of the target point, z. More specifically, it is determined by the number of reflecting boundaries which exist between these points, which we denote N. This gives:

$$R = (-1)^N \tag{7}$$

Referring again to Fig. 2, virtual sources are shown in each of the three regions separated by a reflecting boundary, as well as their nonlinear contributions to the target point at the receiver. For the source in the first region, labelled (1), its nonlinear contribution passes through two boundaries on route to the target, and so the net reflection correction is +1. The contribution from the second source (2) passes through one boundary, and hence its contribution has a correction of -1. The final source (3) is in the same region as the target, its correction is therefore +1. It should be noted that although the linear field is also subject to sign changes between the regions, the virtual nonlinear source amplitudes are proportional to its square, and hence this has no effect.

4 Experimental Results

In order to validate the predictions of the reflection model, a practical test was devised. In essence, the aim was to transmit pulses into a sample and measure the linear and nonlinear responses on both sides of the sample after subsequent reflections - a combined pulse-echo and through-transmission inspection. While in general, the through-transmission part of this would pose no direct challenge, there are problems presented by the pulse-echo measurement. Specifically, it is difficult to use the same device as both a transmitter at the fundamental frequency and a receiver at the second harmonic frequency. In the through-transmission case, generally two different devices are used with frequency responses appropriate to their intended range of use. These can of course also be axially aligned to ensure measurement at the centre of the field. In the pulse-echo case however, using two different sensors on the same surface would usually prevent axial alignment, as the receiver would have to be located adjacent to the transmitter. As a solution to this problem, a ring-shaped piezoelectric disc was used as the transmitter, allowing a receiving probe to be accommodated within its inner radius. Examples of other uses of this approach can be found in Refs. [8, 9, 32].

A schematic illustrating the experimental setup is shown in Fig. 3. The sample used was a cylinder of aluminium of length 20.2 cm and radius 11.4 cm. The transmitting disc (Noliac, N41) had dimensions 10 mm, 25 mm and 4 mm for the inner diameter, outer diameter and thickness, respectively, and was bonded to the surface of the aluminium using a high-strength retaining adhesive. 30-cycle tone burst signals were generated by a computer-controlled digital oscilloscope (Handyscope HS3, Tiepie Engineering) before being amplified and transmitted through the PZT into the sample. At either end of the sample, a wide band probe (Panametrics, 0.25") was used to record the reverberations of the signal inside the specimen and transmit the voltage data, via the handyscope, to the PC for signal processing. A total of five repeat measurements were made at each

of four different frequencies, in between which the receiving probe was removed, and both coupled surfaces were cleaned of coupling gel.

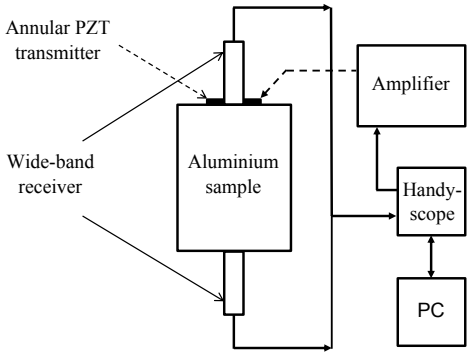

Figure 3: Schematic illustratrating the experimental setup.

The data from the two receiving probes was combined to construct a trend of the amplitude variation at successive reflection points. Data were taken at fundamental frequencies of 2.93, 4.11, 5.27 and 6.43 MHz, which corresponded to peaks in the frequency response of the ring transmitter. The centre frequency of the receiving probe was selected (from 5 or 10MHz) so as to most efficiently capture energy at the second harmonic frequency. The results are shown in Figs. 4 - 7 for each fundamental frequency in turn, where the first two pulses captured on each side of the sample are considered. The upper panels show the fundamental amplitudes, while the lower panels show the second harmonic amplitudes. The measured data are represented by the starred points, where the error bars indicate two standard deviations from the mean of the five measurements. It is pointed out that no calibration was carried out to convert the ultrasonic voltages into amplitude values. This is because the trend of the points, rather than the actual displacement values, was deemed to be the feature of greatest interest.

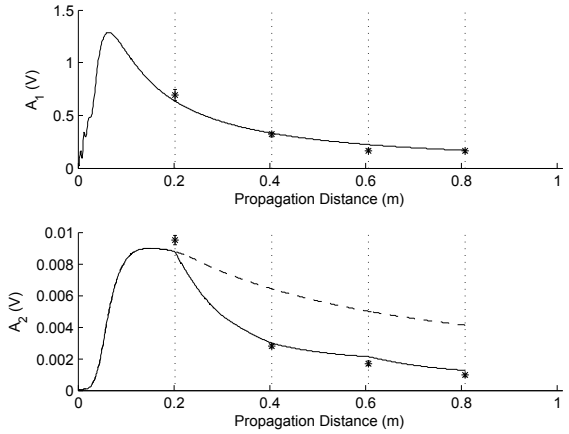

Figure 4: Measured fundamental (upper panel) and second harmonic (lower panel) amplitudes for a source excitation frequency of 2.93 MHz - starred points. The simulated free boundary trends are shown by the solid lines; the dashed line shows the corresponding trends with rigid boundaries. The vertical dotted lines indicate the reflection points.

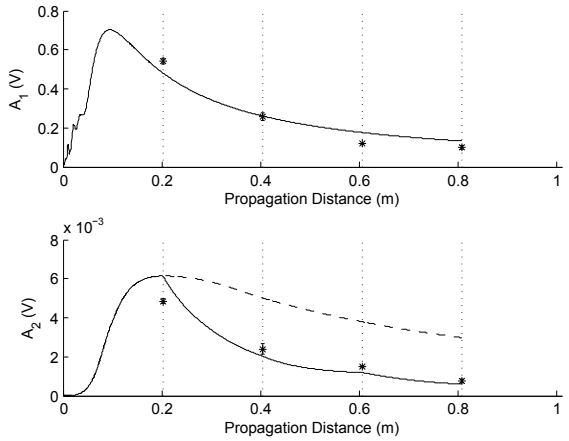

Figure 5: As in Fig. 4, but with fundamental excitation frequency of 4.11 MHz

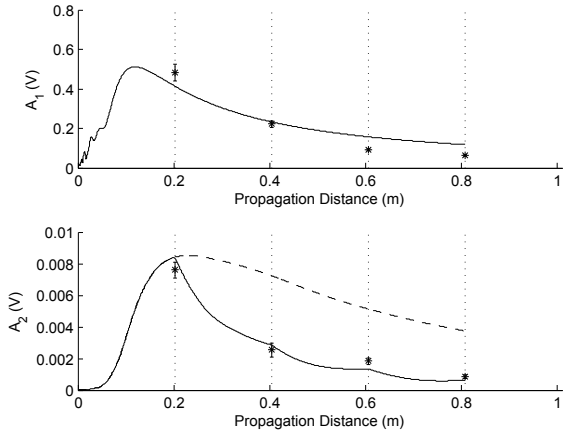

Figure 6: As in Fig. 4, but with fundamental excitation frequency of 5.27 MHz

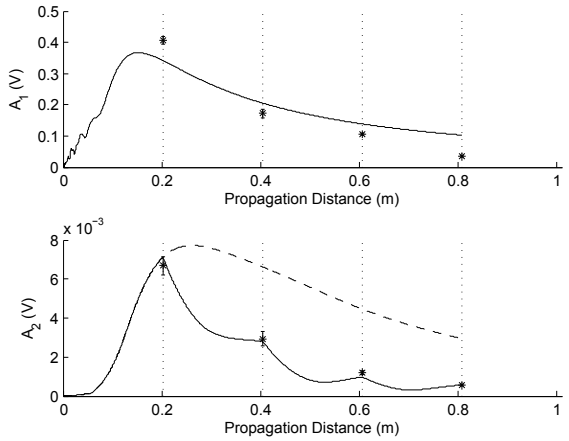

Figure 7: As in Fig. 4, but with fundamental excitation frequency of 6.43 MHz

Superimposed on the measured data are the predictions of the numerical simulation (solid lines), where the input parameters were matched to those of the experiment. This required using appropriate integration limits for the Rayleigh-Sommerfeld integral in order to account for the annular source, while the receiver radius was set to that of the wide-band probe - see Eq. (5). The attenuation coefficients at the fundamental and second harmonic frequencies in the aluminium sample were measured previously by comparing modelled fundamental axial trends with pulse-train data and iterating the attenuation level to find a best fit. As the source amplitude levels and nonlinearity in the medium were not known, each was set to unity in the simulations; both sets of trends were then scaled to provide a weighted mean best fit with the experimental data. To illustrate the effect of the free boundaries, we have also shown - using dashed lines - the corresponding simulated trends with rigid boundaries present (i.e. $R = 1$ is fixed). Note that this is equivalent to through-transmission over the same total propagation distance.

Overall, there is a good level of agreement between the theoretical and measured data over the range of frequencies tested. The variability which exists in the data points (indicated by the error bars) is presumably due to the coupling conditions between the receiver and the surface of the sample, which would have varied slightly for each repeat measurement. Importantly, the signal-to-noise ratio was measured for each of the four points per subplot, and was found to be above 6dB in all cases. This fact was used to confirm that the observed lower amplitudes, in particular those seen in A_2 towards the end of the sequence, were in fact 'real'. A point of interest in the simulated trends is that between reflections, A_2 appears to rise and fall more steeply at higher frequencies, presumably as a result of the higher attenuation levels.

As a final remark, it is pointed out that a measurement of absolute β could be made from the data by running the appropriate simulations with a value of $\beta = 1$, then scaling the resulting trends to fit the measured data. This would of course require that the measured voltages be converted to absolute amplitudes by way of a calibration. Examples of β measurement by similar methods can be found elsewhere, including the aforementioned work [5] and references therein.

5 Optimisation I - Excitation Frequency

As shown in Figs. 4-7, a large drop occurs in the amplitude of the second harmonic between the first and second reflection points. In order to make reliable measurements, it is important that the detectable second harmonic amplitude is as large (with respect to the noise levels) as possible. The question therefore arises as to how a pulse-echo setup may be configured so as to maximise this amplitude.

By rearranging Eq. (1) for A_2, the second harmonic in the through-transmission plane wave scheme is expressed in terms of the other relevant parameters. When all other parameters are fixed, A_2 is directly proportional to k^2, which would suggest that in theory, one could maximise A_2 by maximising k. Considering now the three-dimensional case of a sound beam, this becomes a more complicated relationship, as increasing k pushes the effective range of the near field further away from the source. Therefore, although the k^2 term still exists in the proportionality factor (see Eq. 2), this may be counteracted if the measurement location coincides with a pressure trough amid the near field fluctuations. Moving to the pulse-echo case, this is complicated even further by the presence of a reflecting boundary, and a clear relationship between A_2 and k is not immediately obvious.

To assess the combined effect of these factors, an iterative simulation was conducted to assess the frequency dependence of the reflected linear and second harmonic amplitudes under idealised conditions. Fig. 8 shows the results of this simulation, where the variations of the round-trip A_1 and A_2 are plotted against excitation frequency. The transmitter dimensions and sample length

are matched to those used in the experimental setup, described in the previous section. The two unknown parameters, U_0 and β are fixed to typical values of 10^{-9}m and 5, respectively. The simulation is run for a range of excitation frequencies between 1 and 7 MHz, while the round-trip amplitudes - assumed to be received by a point at the centre of the source - are recorded at each frequency.

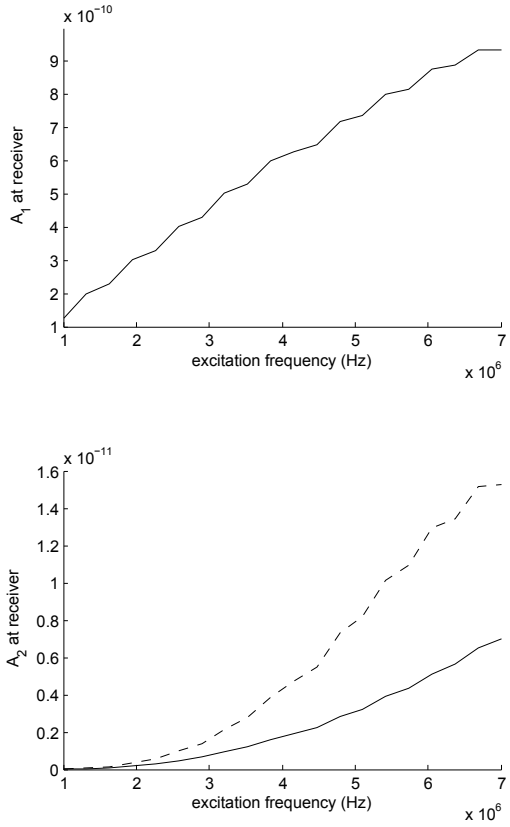

Figure 8: Round-trip fundamental (upper panel) and second harmonic (lower panel) amplitudes vs excitation frequency. The solid lines represent the free-boundary amplitudes, the dashed line in the lower panel shows the rigid boundary equivalents. The boundary distance is $z_{bound} = 0.202$m.

The round-trip A_1 are shown in the upper panel, and increase monotonically over the range of frequencies. This is due to the final amplitude maximum in the sound beam being pushed further out at the higher frequencies, such that is it closer to the point of reception. In the lower panel, the solid line indicates the round-trip A_2 in the presence of a free boundary, while the dashed line shows the corresponding trends when the boundary is rigid (equivalent to through-transmission over a double-length medium). As expected, at all frequencies in the range, the rigid boundary amplitudes are larger than the free boundary equivalents, and increase monotonically. Of greater practical relevance is the fact that the free boundary amplitudes also appear to increase monotonically with excitation frequency. This indicates that, similarly to the plane wave case, the k^2 dependence remains the dominant factor in determining the magnitude of A_2 when both three dimensionality and free boundaries are included. Theoretically therefore, it is possible that in both the pulse-echo and through-transmission configurations, nonlinear amplitudes could be maximised by using as high an excitation frequency as possible.

A qualifying point here is that for the simulation shown, the sample length, $z_{bound} = 0.202$m, is such that even at the highest inspection frequency of 7 MHz, the near-field region of the sound beam does not extend to the point of reception at $z = 0.404$m. As such, Fig. 8 effectively shows the excitation frequency dependence of the far-field amplitudes. In the alternative case where the point of reception coincides with the near field of the beam, the received amplitude is likely to be determined to a greater extend by the positions of the peaks and troughs in this region. The effect of increasing excitation frequency may therefore be somewhat different. In order to investigate this, a second simulation was run with identical parameters to the previous one, only now with the sample length set to $z_{bound} = 0.020$m, roughly a tenth of that previously.

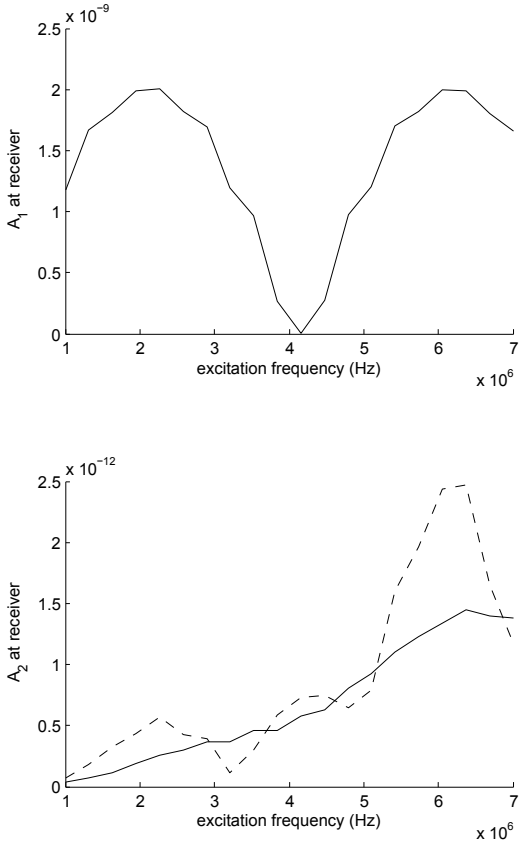

Figure 9: As in Fig. 8, but now with $z_{bound} = 0.020$m.

The A_1, shown in the upper panel, now behave rather differently. An oscillating pattern can be seen which reflects the outward movement of the near field peaks and troughs with increasing excitation frequency. This oscillation is also seen to an extent in the rigid boundary A_2, shown by the dashed line in the lower panel. Here the increase is no longer monotonic with frequency, instead there is a pronounced minimum occuring just beyond 3 MHz, slightly before the minimum in A_1. This is expected, as the last near field minimum in the second harmonic beam occurs spatially after that of the fundamental beam. The trend then shows a general increase before a second drop at around 6.5 MHz, which also reflects a corresponding drop in A_1. The free boundary A_2 trend on the other hand, indicated by the solids line in the lower panel, appears once again to increase almost monotonically with frequency. An explanation for this is that the free boundary effectively reverses

the phase interferences which lead to the natural diffractive near field behaviour. This smoothing effect means that more nonlinear contributions beyond the boundary add in phase, leading to a steady increase. Notably, at certain points in the frequency range, the free boundary A_2 are actually larger than the rigid boundary equivalent.

Overall, this suggests that when making pulse-echo measurements with a free boundary, there may be nonlinear amplitudes gains to be exploited by using higher frequencies, whether the measurement takes place in the near or far field of the beam. In the case of a rigid boundary (or a though-transmission measurement), the case is the same in the far field, but more care should be taken when measuring in the near field. It is pointed out that these conclusions are relevant only when all parameters other than the excitation frequency are considered equal. This becomes important when considering that most experimental equipment will be limited in its range of operational frequencies, and that its response over this range, either for transmission or reception, will not be uniform. Furthermore, operation at very high frequencies may be restricted by noise and sampling rate issues. Attenuation levels, sample and transmitter/receiver dimensions specific to a particular setup would also need to be taken into account.

6 Optimisation II - Focused Excitation

Another way of addressing the problem of optimising pulse-echo measurements is to consider the use of focusing acoustic sources. It is thought that by using a beam focused at a virtual point beyond the free boundary, this would force the majority of the nonlinear generation to take place after reflection. This may then partially alleviate the problem of having cancelling second harmonic contributions. An additional advantage is that, in the focal region, a focused source is known to generate a much larger amplitude second harmonic signal than an unfocused beam with the same frequency and source excitation level. Recent related work in the field of fluids includes that of Saito et al. [10, 11], who used focused sources to make nonlinearity measurements in fluids using a submerged reflector. In this case, appropriate positioning of the reflector enabled the maximum nonlinear amplitude to be received by the focused Gaussian source. Here we described the incorporation of beam focusing into the numerical model described in Section 2.

The solution for a focused acoustic source with continuous sinusoidal excitation was derived earlier by O'Neil [33] using the Rayleigh integral approximation. The assumption therein is that the frequency of vibration is sufficiently high that radiation from a source element is not significantly diffracted by the neighbouring elements. (Note that the assumption of large ka is one also made in the model described in Section 2). Each source element on the curved surface is therefore assumed to radiate a spherical wave, enabling summation by the Rayleigh integral. In more recent work, Hamilton [34] compared the result of this approach (see his Eq. (2)) with other results found by using first a planar source condition assumption, and then using the parabolic approximation - each method was shown to produce a similar result. Here we take the Rayleigh integral approach and use an adapted algorithm, similar to that used previously [20], to solve the integral numerically. This makes a relatively simple incorporation into the full nonlinear model, which is otherwise as described in Section 2.

The aim is to determine the optimal focal position of a beam emitting into a medium with a pressure-release boundary, with a view to maximising the received second harmonic. In order to focus a beam within a certain distance, the source excitation must be selected accordingly. This is because the maximum focal distance of a source is in part determined by its excitation frequency. The acoustic focal distance of the beam, D_{ac}, is different to the geometrical (or optical) focal distance, D_{opt} - see for example [34]. Specifically, as D_{opt} increases to infinity, D_{ac} tends towards the

Fresnel distance of the beam, which roughly corresponds to the position of the last amplitude maximum. Therefore, in order to enable a true acoustic focal point within a distance z, the excitation condition must be set such that the Fresnel distance is larger than z.

In order to determine the effect of changing focal distance, a iterative simulation similar to those described previously was run. In keeping with the previous simulation, the input parameters here are set to match those of Fig. 9. That is, the transmitter dimensions are matched to those of the experiment in Section 4, the source excitation and medium nonlinearity are set to $U_0 = 10^{-9}$ m, $\beta = 5$ respectively, and the smaller sample length of $z_{bound} = 0.020$ m is used. The excitation frequency of the annular source is therefore set to 7 MHz in order to ensure positioning of the Fresnel distance beyond $2z_{bound}$. Fig. 10 shows the received round trip fundamental amplitudes (upper panel) and second harmonic amplitudes (lower panel) when the optical focal distance of the beam is varied between $(0.015 \text{ m} \leq D_{opt} \leq 0.045 \text{ m})$, or $(0.75 \leq (D_{opt}/z_{bound}) \leq 2.25)$.

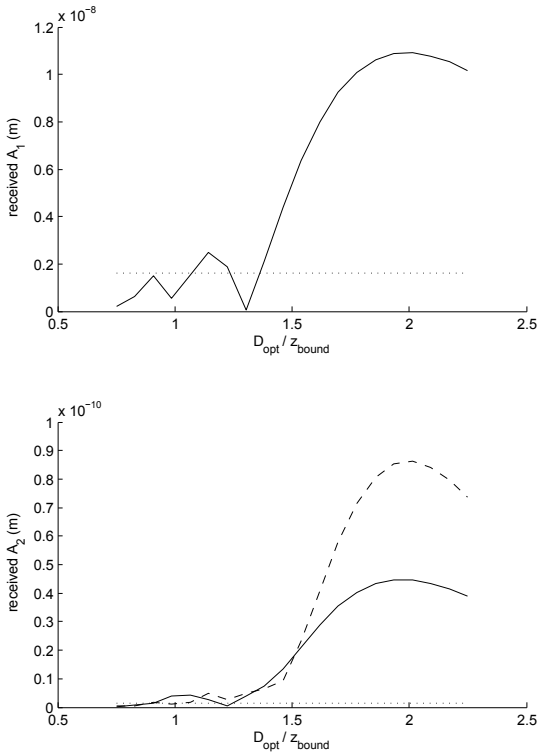

Figure 10: Round-trip free boundary linear (upper panel) and nonlinear (lower panel) amplitudes vs. (D_{opt}/z_{bound}), shown by the soild lines: The dashed line represents the equivalent rigid boundary A_2. The sample length is $z_{bound} = 0.020$ m.

The round-trip free boundary amplitudes are shown by the solid lines, while the dashed line in the lower panel shows, as previously, the equivalent rigid boundary amplitudes. The horizontal dotted line in each panel represents the equivalent free boundary round-trip amplitude from an unfocused beam with otherwise identical excitation parameters.

The value of A_1 oscillates in the first portion of the range before increasing to a maximum just before $D_{opt} = 2z_{bound}$, which is as expected, as here the beam is directly focused at the point of reception. In the lower panel, the nonlinear amplitudes A_2 show similar behaviour, with both rigid and free boundary amplitudes peaking at roughly $D_{opt} = 2z_{bound}$. The higher rigid boundary

amplitudes are expected as there is no obstacle affecting the nonlinear accumulation. For most of the range, both sets of focused amplitudes are significantly higher than the unfocused amplitudes - shown by the horizontal dotted line. Overall, these results suggest that focusing the beam at roughly $z = 2z_{bound}$ may be optimal in terms of maximising the round trip nonlinear amplitude. However, focusing before, or even after this point, may also provide a significant gain in A_2 compared to the unfocused case.

The potential of using a focused source should be put into context. Due to the beam features discussed earlier, it is likely that inspection of an object of a certain length will probably require an operational frequency within a certain range, and/or certain transmitter dimensions. Also, manipulation of the acoustic focal depth will probably not be possible in a fixed-range device. However, here we can envisage the use of phased array devices, which would enable a greater degree of flexibility both in transmission and reception.

7 Conclusions

In this paper we have investigated the feasibility of making pulse-echo harmonic generation measurements with a view to non-destructive evaluation applications. A numerical model has been developed which addresses the process of nonlinear generation in a three-dimensional sound beam in the quasi-linear regime. The model can be used to simulate any source excitation condition with axial symmetry, and incorporates the the effects of multiple reflecting boundaries within the propagation domain.

A series of results were presented from an experimental test designed to measure the nonlinear generation in the presence of multiple free boundaries. The test measured the changes in second harmonic amplitude of a signal undergoing multiple round trips within a specimen. Experimental data were compared with the predicted results of the simulation, up to the point of the fourth reflection, and were found to be in reasonably good agreement. Futhermore, the results demonstrated that, contrary to previous theoretical indications based on plane wave analysis, detectable nonlinearity is possible beyond the point of first reflection, at least up until the points of third and fourth reflection.

Using similar parameters to those of the experiment, an analysis of the effects of excitation frequency on measurable nonlinear amplitude was then conducted by way of a numerical simulation. Here it was found that the received (round-trip) second harmonic amplitude increased almost monotonically with the value ka of the source excitation. This indicates that, in the pulse-echo configuration, it may be beneficial to use as high an excitation frequency as possible in order to maximise the detectable second harmonic amplitudes.

The effect of beam focusing was then considered using the same numerical framework. Simulations showed that a focusing source can provide a significant gain in nonlinear amplitude when compared to an unfocused source with otherwise identical excitation parameters. Additionally, it was shown that the amplitude could be further maximised by fine-tuning the depth of focus within the region of two times the boundary distance.

In summary, we have shown that pulse-echo harmonic generation measurements could indeed provide a viable, more practical alternative to the through-transmission type. Experimental results have shown that detectable nonlinearity is achievable even after the inspection signal has completed multiple round trips of a specimen. Further to this, numerical simulations have indicated that it may be possible to optimise certain experimental parameters in order to increase the detectable nonlinear signal amplitudes.

References

[1] S. Baby, B. N. Kowmudi, C. M. Omprakash, D. V. V. Satyanarayana, K. Balasubramaniam, and V. Kumar. Creep damage assessment in titanium alloy using a nonlinear ultrasonic technique. *Scripta Materialia*, 59(8):818–821, 2008.

[2] J.-Y. Kim, L. J. Jacobs, J. Qu, and J. W. Littles. Experimental characterization of fatigue damage in a nickel-base superalloy using nonlinear ultrasonic waves. *Journal of the Acoustical Society of America*, 120(3):1266–1273, 2006.

[3] A. Kumar, C. J. Torbet, T. M. Pollock, and J. W. Jones. In situ characterization of fatigue damage evolution in a cast Al alloy via nonlinear ultrasonic measurements. *Acta Materialia*, 58(6):2143–2154, APR 2010.

[4] J.H Cantrell and W.T. Yost. Nonlinear ultrasonic characterization of fatigue microstructures. *International Journal of Fatigue*, 23, Supplement 1(0):487 – 490, 2001.

[5] S.R. Best, A.J. Croxford, and S.A. Neild. Modelling harmonic generation measurements in solids. *Ultrasonics*, (0):–, 2013.

[6] Greer S. Garrett, Jacqueline Naze Tjotta, Richard L. Rolleigh, and Sigve Tjotta. Reflection of parametric radiation from a finite planar target. *The Journal of the Acoustical Society of America*, 75(5):1462–1472, 1984.

[7] Xiufen Gong, Dong Zhang, Jiehui Liu, Huanlei Wang, Yongsheng Yan, and Xiaochen Xu. Study of acoustic nonlinearity parameter imaging methods in reflection mode for biological tissues. *The Journal of the Acoustical Society of America*, 116(3):1819–1825, 2004.

[8] T. Christopher. Experimental investigation of finite amplitude distortion-based, second harmonic pulse echo ultrasonic imaging. *Ultrasonics, Ferroelectrics and Frequency Control, IEEE Transactions on*, 45:158–162, 1998.

[9] Ahmed Chitnalah, Djilali Kourtiche, Hicham Jakjoud, and Mustapha Nadi. Pulse echo method for nonlinear ultrasound parameter measurement. *Electronic Journal - Technical Acoustics*, page 13, 2007.

[10] Shigemi Saito, Jung-Ho Kim, and Kiyoshi Nakamura. Automatic measurement of the nonlinearity parameter b/a in liquid media. *Ultrasonics*, 44, Supplement(0):e1429 – e1433, 2006. Proceedings of Ultrasonics International and World Congress on Ultrasonics.

[11] Shigemi Saito. Nonlinearly generated second harmonic sound in a focused beam reflected from free surface. *Acoustical Science and Technology*, 26(1):55–61, 2005.

[12] E. A. Zabolotskaya and R. V. Kokhlov. Quasi-plane waves in the nonlinear acoustics of confined beams. *Sov. Phys. Acoust.*, 15:35–40, 1969.

[13] V. P. Kuznetsov. Equations of nonlinear acoustics. *Sov. Phys. Acoust.*, 16:467–470, 1971.

[14] Yang-Sub Lee and Mark F. Hamilton. Time-domain modeling of pulsed finite-amplitude sound beams. *The Journal of the Acoustical Society of America*, 97(2):906–917, 1995.

[15] S.I. Aanonsen, T. Barkve, J. Naze Tjøtta, and S. Tjøtta. Distortion and harmonic generation in the nearfield of a finite amplitude sound beam. *Journal of the Acoustical Society of America*, 75:749–768, 1984.

[16] Jarle Berntsen, Jacqueline Naze Tjotta, and Sigve Tjotta. Nearfield of a large acoustic transducer. part iv: Second harmonic and sum frequency radiation. *The Journal of the Acoustical Society of America*, 75(5):1383–1391, 1984.

[17] M. F. Hamilton. *Nonlinear Acoustics, Chapter 8: 'Sound Beams'*. Academic Press, 1998.

[18] F. Ingenito and A. O Williams Jr. Calculation of second-harmonic generation in a piston beam. *The Journal of the Acoustical Society of America*, 49(1B):319–328, 1971.

[19] R. T. Beyer. *Nonlinear Acoustics, Chapter 2: 'The Parameter B/A'*. Academic Press, 1998.

[20] J. Zemanek. Beam behavior within the nearfield of a vibrating piston. *The Journal of the Acoustical Society of America*, 49(1B):181–191, 1971.

[21] A. O. Williams Jr. The piston source at high frequencies. *The Journal of the Acoustical Society of America*, 23(1):1–6, 1951.

[22] P. H. Rogers and A. L. Van Buren. An exact expression for the lommel-diffraction correction integral. *The Journal of the Acoustical Society of America*, 55(4):724–728, 1974.

[23] R. D. Fay. Oppositely directed plane finite waves. *The Journal of the Acoustical Society of America*, 29(11):1200–1203, 1957.

[24] M. A. Breazeale and W. W. Lester. Demonstration of the "least stable waveform" of finite amplitude waves. *The Journal of the Acoustical Society of America*, 33(12):1803–1803, 1961.

[25] D. O. Thompson, M. A. Tennison, and O. Buck. Reflections of harmonics generated by finite-amplitude waves. *The Journal of the Acoustical Society of America*, 44(2):435–436, 1968.

[26] A. L. Van Buren and M. A. Breazeale. Reflection of finite-amplitude ultrasonic waves. i. phase shift. *The Journal of the Acoustical Society of America*, 44(4):1014–1020, 1968.

[27] A. L. Van Buren and M. A. Breazeale. Reflection of finite-amplitude ultrasonic waves. ii. propagation. *The Journal of the Acoustical Society of America*, 44(4):1021–1027, 1968.

[28] O. Buck and D. O. Thompson. Relation of finite amplitude waves to third order elastic constants. *Materials Science and Engineering*, 1(2):117 – 140, 1966.

[29] Frank A. Bender, Jin-Yeon Kim, Laurence J. Jacobs, and Jianmin Qu. The generation of second harmonic waves in an isotropic solid with quadratic nonlinearity under the presence of a stress-free boundary. *Wave Motion*, 50(2):146 – 161, 2013.

[30] Jacqueline Naze Tjotta and Sigve Tjotta. An analytical model for the nearfield of a baffled piston transducer. *The Journal of the Acoustical Society of America*, 68(1):334–339, 1980.

[31] Inder Raj S. Makin, Michalakis A. Averkiou, and Mark F. Hamilton. Second-harmonic generation in a sound beam reflected and transmitted at a curved interface. *The Journal of the Acoustical Society of America*, 108(4):1505–1513, 2000.

[32] Ping Wu and T. Stepinski. Ultrasonic harmonic imaging in nondestructive evaluation: preliminary experimental study. *Ultrasonics Symposium, 2000 IEEE*, 1:801–804, 2000.

[33] H. T. O'Neil. Theory of focusing radiators. *The Journal of the Acoustical Society of America*, 21(5):516–526, 1949.

[34] Mark F. Hamilton. Comparison of three transient solutions for the axial pressure in a focused sound beam. *The Journal of the Acoustical Society of America*, 92(1):527–532, 1992.